Simultaneous electrochemical determination of benzenediol compounds in environmental samples using nano architectures of hydrogen ammonium zinc molybdate layered double hydroxides integrated with carbon black modified electrode

Chelladurai Karuppiah[a#], Sivakumar Musuvadhi Babulal[b#], Shen-Ming Chen[b*], Selvakumar Palanisamy[c*], Li-Fan Hsu[a], Chun-Chen Yang[a,d,e*], Matteo Chiesa[c, f*],

[a]Battery Research center of Green Energy, Ming Chi University of Technology, New Taipei City 24301, Taiwan, R.O.C.

[b]Electroanalysis and Bioelectrochemistry Lab, Department of Chemical Engineering and Biotechnology, National Taipei University of Technology, No.1, Section 3, Chung-Hsiao East Road, Taipei 106, Taiwan R.O.C.

[c]Laboratory for Energy and NanoScience (LENS), Khalifa University of Science and Technology, Masdar Campus, PO Box, 54224, Abu Dhabi, United Arab Emirates.

[d]Department of Chemical Engineering, Ming Chi University of Technology, New Taipei City 24301, Taiwan, R.O.C.

[e]Department of Chemical and Materials Engineering, Chang Gung University, Taoyuan City 333, Taiwan, R.O.C.

[f]Department of Physics and Technology, UiT The Artic University of Norway, 9010, Tromso, Norway.

#These authors equally to this work

*Corresponding Authors:

*S-M Chen, **Email:** smchen78@ms15.hinet.net; S.Palanisamy, **Email:** prmselva@gmail.com; selvakumar.palanisamy@ku.ac.ae; C-C Yang, **Email:** ccyang@mail.mcut.edu.tw; M. Chiesa, **Email:** matteo.chiesa@ku.ac.ae

Abstract

Phenolic compounds, including benzenediol (BD), are toxic and poorly biodegradable, so even at shallow levels, they can pose a threat to health and the environment. Therefore, the simultaneous detection of BD at low detection limits with a wide detection range is of significant interest for monitoring water quality and environmental remediation. In the present work, a novel BD electrochemical sensor was fabricated based on a hydrogen ammonium zinc molybdate layered double hydroxide (AZnMo-LDHs) coupled carbon black (CB) nanocomposites (NC) modified electrode. The morphological, structural, and physical-chemical properties of AZnMo-LDHs/CB NC were verified by various characterization methods. The NC-modified electrode had low electrical resistance, high electrocatalytic activity, and fast electron transport due to the synergy between AZnMo-LDHs and CB. Also, the NC-modified electrode provided excellent electrochemical performance for selective and simultaneous determination of hydroquinone (HQ), catechol (CC), and resorcinol (RC). Differential pulse voltammetric studies confirmed that AZnMo-LDHs/CB NC could detect HQ, CC, and RC in the linear response ranges of 0.05-971, 0.1-1036, and 0.5-1408.5 μM, respectively, with detection limits of 0.0054, 0.0018, and 0.075 μM. The proposed sensor was tested in multiple environmental samples, including water and soil, and showed an excellent recovery of HQ, CC, and RC.

Keywords: Layered double hydroxides, conductive carbon black, voltammetric detection, benzenediol, environmental sample analysis

1. Introduction

It is common for phenolic compounds to be included in the list of the world's most polluted water bodies because they are toxic and harmful to the liver and nervous system [1]. Among phenolic compounds, dihydroxybenzene isomers (DBi) such as hydroquinone (HQ), catechol (CC), and resorcinol (RC) have found extensive applications in medicine, paint, and organic chemical synthesis [2–4]. The European Union (EU) and US Environmental Protection Agency (EPA) consider DBi to be potent environmental pollutants, owing to their non-biodegradability and toxic nature, causing environmental pollution and harming living creatures [5]. So far, traditional methods (spectrophotometry, high-performance liquid chromatography, and electrochemiluminescence) and electrochemical detection methods have been used in the detection DBi [6–9]. Electrochemical methods offer high sensitivity, precision, and simple equipment producers compared to earlier traditional spectrophotometric and chromatographic techniques [9]. Given the close structures and chemical characteristics of DBi, the electrochemical method can be used for selective detection of HQ, CC, and RC. Unmodified electrodes are unsuitable for electroanalysis of DBi due to their overlapping oxidation peak potentials of HQ and CC. The above issue was resolved using chemically modified electrodes to distinguish the peak oxidation potentials and enhance HQ, CT, and RC signals. However, the complex electrooxidation reaction of DBi makes it challenging to design a sensor for selective and simultaneous detection of HQ, CC, and RC.

In materials science, a metal mixed-metal hydroxide is a layered double hydroxide (LDH) characterized by a periodicity at nanometer scales [10]. It has therefore received considerable attention because of its full charge separation between layers and galleries and its periodicity [10,11]. These materials are widely used in various applications, including electrochemical sensors, due to their characteristics and inherent electrocatalytic properties [11,12]. In recent years, transition metal-based LDHs have been synthesized using various methods, and their electrochemical applications have attracted significant attention. For instance, hydrothermal and co-precipitation methods are widely used to synthesize Co-Ni, Co-Zn, and Co-Mo-based

LDHs for supercapacitors, oxygen reduction reactions, and electrochemical sensors [12]. For example, hydrogen zinc molybdate layered double hydroxides (AZnMo-LDHs) have excellent electro-optical and magnetic properties due to their multiple stable oxidation states [13–14]. Due to their excellent electrocatalytic properties coupled with durability, low cost, calcination-free, and flexibility, AZnMo-LDHs have excellent electrocatalytic properties and are eco-friendly and highly durable [15]. AZnMo-LDHs are ideally suited for electrochemical sensor applications due to their high surface activity, high conductivity, and rapid charge transfer characteristics. It is relevant to note that LDHs tend to aggregate and self-stick when used as electrodes, and their size distribution is uneven with irregular geometries [16]. To address the above problems, carbon nanomaterials can be hybridized with LDHs to create new types of nanohybrid LDHs for electrochemical sensor applications. Graphene, carbon dots, and carbon nanotubes are excellent candidates for functionalization with LDHs due to their benefits, such as electrical conductivity, mechanical strength, thermal stability, and electrocatalytic properties [17–19]. One of these is carbon black (CB), characterized by mainly hybridized sp^2 carbon atoms with a few sp^3 carbon atoms and graphite-like crystals arranged in the reticulate chain or branch configurations [20]. The zero-dimensional (0D) CB is an excellent candidate and has the following advantages: a low aspect ratio, a low cost (relative to graphene and CNTs), and good conductivity [20]. In addition, it has unique physicochemical properties; CB can quickly produce a stable dispersion in various solvents, including aqueous solutions [21]. We used CB despite this because of its high conductivity and because its addition preserves the nanostructure of LDHs while improving their stability. As a result of these remarkable properties of the CB, composite materials have been developed for various electrochemical sensor applications [22–27]. In addition, a superlattice composite structure consisting of 2D LDHs and 0D conductive CBs can provide a synergistic effect in electrocatalysis and enhance electron transfer efficiency. As far as we know, this is the first work combining 2D AZnMo-based LDHs and 0D CB as AZnMo-LDHs/CB nanocomposite (AZnMo-LDHs/CB NC) electrode materials for electrochemical sensors applications.

This work presents a simple and low-cost approach to fabricating AZnMo-LDHs/CB NC-based selective and sensitive electrochemical DBi sensors. The AZnMo-LDHs nanoflakes (AZnMo-LDHs NFs) were synthesized using a co-precipitation method, and the AZnMo-LDHs/CB NC was prepared by a wet chemical-assisted method. Using the analytical instrumentation of cyclic voltammetry (CV) and differential pulse voltammetry (DPV), HQ, CC, and RC were simultaneously detected by the AZnMo-LDHs/CB NC modified GCE. The kinetics of redox reactions were also evaluated by studying scan rate and pH variations. We evaluated the practical application of the sensor using several waters and soil samples.

2. Experimental section

2.1. Materials and apparatus

$Zn(NO_3)_2.6H_2O$, ≥99%, $(NH_4)_6Mo_7O_{24}.4H_2O$, ≥99%, NaOH, ≥98%, HCL, 37%, NaH_2PO_4, ≥99%, Na_2HPO_4, ≥99%, hydroquinone (≥99.5%), 1,2-dihydroxybenzene (≥99.5%) and resorcinol (≥99%), were obtained from the Sigma Aldrich company. The electroanalysis and electrocatalytic experiments were conducted using modified glassy carbon electrodes (GCEs) as working electrodes with Ag/AgCl (3M KCl) as a reference and platinum wire as a counter electrode. We characterized and evaluated electrochemical performance using electrochemical impedance spectroscopy (IM6ex ZAHNER instrument from Kronach, Germany) and voltammetric methods (CHI1205A, CHI 900 CH Instruments, Austin, TX, USA).

2.2. Preparation of AZnMo-LDHs/CB NC and electrode modifications

AZnMo-LDHs NFs were synthesized using a previously reported method [15]. The as-prepared AZnMo-LDHs (50 mg) and CB (40 mg) were mixed with 50 mL of ethanol. Subsequently, the dispersion solution was kept under ultrasonic irradiation for 1 h. The black color dispersion was continuously centrifugated at 6000 rpm and dried in an air oven at 50 °C for 12 h after being washed with ethanol and water. Finally, the collected

product has been named as AZnMo-LDHs/CB NC and used to further processes (**Scheme 1**). As soon as the NC was prepared, AZnMo-LDHs/CB water dispersion (5 mg/mL) was prepared using the sonication method (1 h). About 5 µL (optimum) of the as-prepared NC was coated on alumina polished GCE and dried at 40 °C. The NC-modified GCE was used for electrochemical sensing applications of DBi using CV and DPV. We prepared AZnMo-LDHs, CB, and AZnMo-LDHs/CB modified GCEs for comparison and measured their electrocatalytic activity against DBi and was performed in a pH 7.0 phosphate buffer solution (PBS).

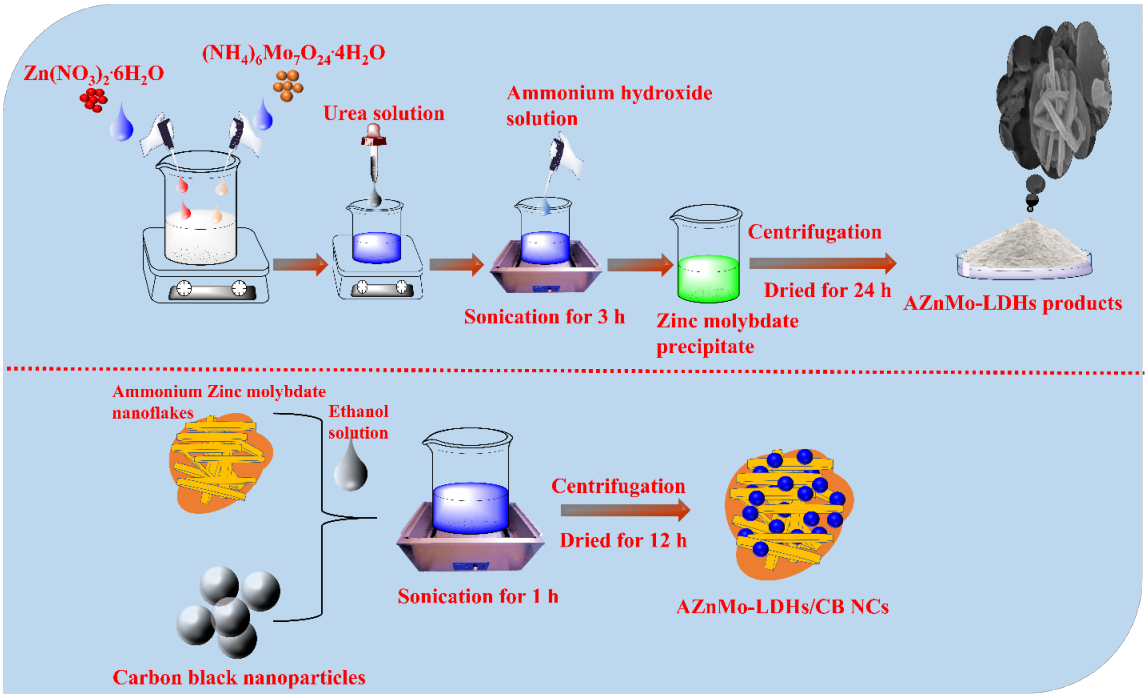

Scheme 1. The schematical illustration for the detailed synthesis procedure of AZnMo-LDHs/CB NC.

2.3. Characterization for AZnMo-LDHs/CB NC

Transmission electron microscopy (TEM) from Shimadzu JEM-1200 EXSTEM, Tokyo, Japan, and the Field emission scanning electron microscopy (FE-SEM) from the JSM-7610F, JEOL were used for the morphology and intrinsic structure analysis of the materials. X-ray diffraction (XRD) analysis for as-prepared materials was studied using Panalytical X'pert PRO MRD, Almelo, Netherlands. The vibrational band disorder of the materials was measured with a micro-Raman Dongwoo Ramboss 500i spectrometer using a laser at 514

nm. The chemical state of elements has been evaluated through X-ray photoelectron spectroscopy (XPS) using the Thermo ESCLAB 250 instrument.

3. Results and discussion

3.1. Morphological analysis

The structure and surface morphologies of AZnMo-LDHs, CB, and AZnMo-LDHs/CB NC were analyzed by FESEM. Fig. S1(a-c) shows different spots with magnifications of 1 μm and 100 nm that confirm the layered double hydroxide morphology of 2D nanoflakes. A vertical alignment and good interrelationship can be seen in the formation of highly accumulated nanoflakes. It is possible that the synthesized nanoflakes-like morphology of the AZnMo-LDHs could play a crucial role in the catalytic reaction on the surface-modified GCEs. It is evident from the higher angle view that the nanoflakes-like morphology of the AZnMo-LDHs exhibits excellent purity. Fig. S1d-f shows FESEM images of CB under lower angles magnification at different locations. According to the FESEM images, the CB are agglomerated into spherical shapes, especially those containing many small nanoparticles. As a result of the aggregated spherical-like CB, we have achieved higher electrical conductivity and a more facile electrochemical reaction activity at the interface between the electrode and electrolyte. Moreover, the FESEM images of AZnMo-LDHs/CB NC are shown in Fig. S1(g-i). Undoubtedly, the flakes-like structures of AZnMo-LDHs are fully occupied (or) integrated within the spherical-like composites of CB, revealing the formation of a 2D/0D composite structure. Our investigation of the fabricated AZnMo-LDHs/CB NC was further enhanced by utilizing FESEM-EDX elemental mapping (Fig. S2 (a-f)). An EDX spectrum confirms the elemental percentage ratio and the full coverage of the individual elements (Zn, Mo, O, and C).

In addition, as-prepared AZnMo-LDHs, CB, and CB NC were examined using TEM. As shown in Fig. 1a-b, the AZnMo-LDHs exhibit a 2D structure morphology with uniform nanoflakes. Additionally, the nanocrystalline AZnMo-LDHs depicting the ultrathin 2D nanoflakes-like structure can be seen in the zoomed

view in Fig. 1b. According to Fig. 1c, CB nanoparticles in the graph have a predominantly spherical shape with aggregations measured at 85 nm (or each primary CB particle measuring 15 nm). Fig. 1d-f illustrates the inter-structural morphology of AZnMo-LDHs and CB. This TEM image displays the different magnification views of the hierarchical morphology of the conducting networks formed by the AZnMo-LDHs nanoflakes integrated with CB nanoparticles. The insert in Fig. 1f shows the SAED pattern of the AZnMo-LDHs/CB NC; it is clearly visible that the CB composition is amorphous in contrast to the crystalline lattice of the AZnMo-LDHs. Consequently, the nanocomposite modified electrode might exhibit facile electrochemical reactivity because of its physicochemical properties while enhancing electrical conductivity, and it may enhance the sensitivities of the electrochemical detection by the nanoparticles integrated on the nanoflakes surfaces.

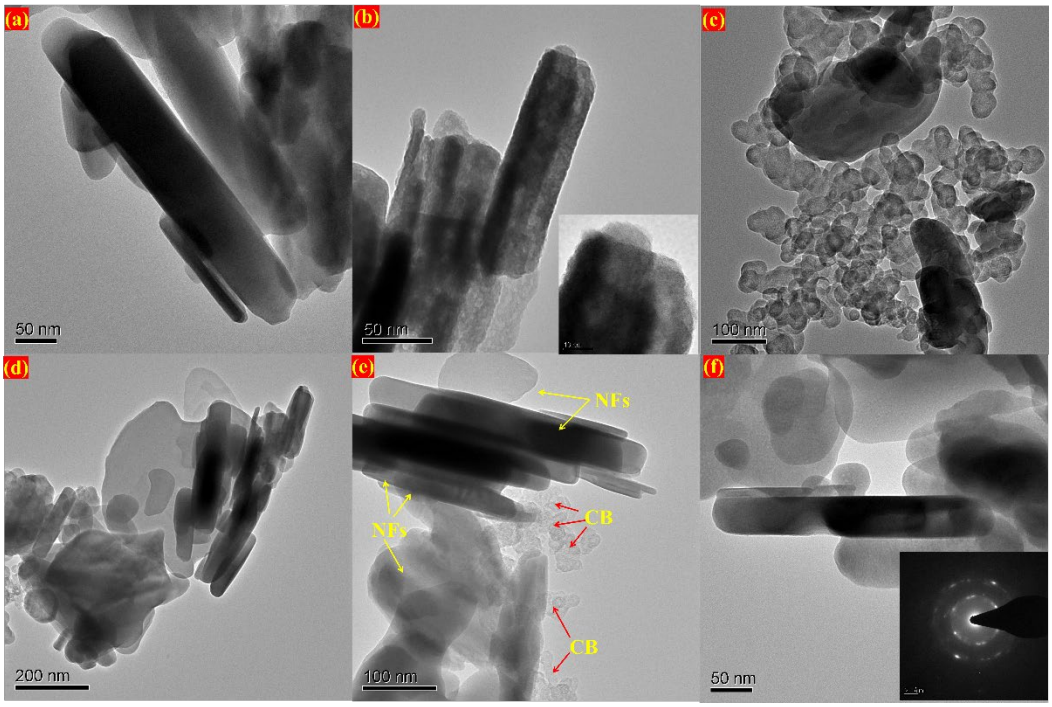

Fig. 1. TEM images of AZnMo-LDHs (a-b), carbon block (c), AZnMo-LDHs/CB NC (d-f), and SAED patterns of the AZnMo-LDHs/CB NC (insert (f)).

3.2. The investigation of crystallinity and bonding vibrational characteristics of AZnMo-LDHs/CB NC

The details of the crystalline formation, phase, and space group of AZnMo-LDHs, CB, and AZnMo-LDHs/CB NC were inspected by XRD analysis as seen in Fig. 2A(a-c). The 2θ values at 12.2°, 17.2°, 18.6°, 23.4°, 24.6°, 26.5°, 29.2°, 31.8°, 33.5°, 34.1°, 34.9°, 37.2°, 38.5°, 45.1°, 48.5°, 50.2°, 54.6°, 54.7°, 58.3°, and 60.6° are attributed to the hydrogen ammonium zinc molybdenum oxide ($H_3NH_4Zn_2Mo_2O_{10}$) formation, Rhombhahedral crystal system, R-3m space group, was demonstrated with previously research publication and clearly matched with the JCPDS card no. 01-73-2389 [28]. Good intensity growth and high purity of the crystal's formation are evident from XRD patterns. The XRD pattern revealed the amorphous nature of the CB, and the diffraction pattern showed 2θ values at 25.3° and 43.5°[29]. The above similar diffraction patterns are observed in the XRD patterns of AZnMo-LDHs/CB NC. Furthermore, no other impurities are present with the peak intensity, and the angle has been modified, which indicates the well-built nanocomposites as shown in Fig. 2A(c). In addition, the micro-Raman spectrum of AZnMo-LDHs, CB, and AZnMo-LDHs/CB NC is shown in Fig. 2B(a-c). Asymmetric and an asymmetric stretching vibration of Mo-O bonds of distorted MoO_4 of zinc molybdate gave rise to the characteristic peaks at 934, 886, and 780 cm^{-1}. The micro-Raman spectra of a band at 340 and 934 cm^{-1} correspond to Mo–O–Zn stretching vibrations and the existence of a tetrahedral molybdate ion, which can be recognized by two distinct bands [28,30–33]. Also, in the micro-Raman spectrum of CB (Fig. 2B(b)), two prominent bands are observed at 1354 and 1600 cm^{-1}, which are associated with disordered structures (D-bands), and their intensity diminishes with increasing graphitic plane size (G-bands); therefore, these data were used to estimate in-plane graphitic crystal dimensions [34,35]. All the functional characteristics are presented in the as-fabricated AZnMo-LDHs/CB NC of the Raman spectrum, as shown in Fig. 2B(c). Based on these findings, the composite fabrication has successfully combined CB nanoparticles with AZnMo-LDHs NFs.

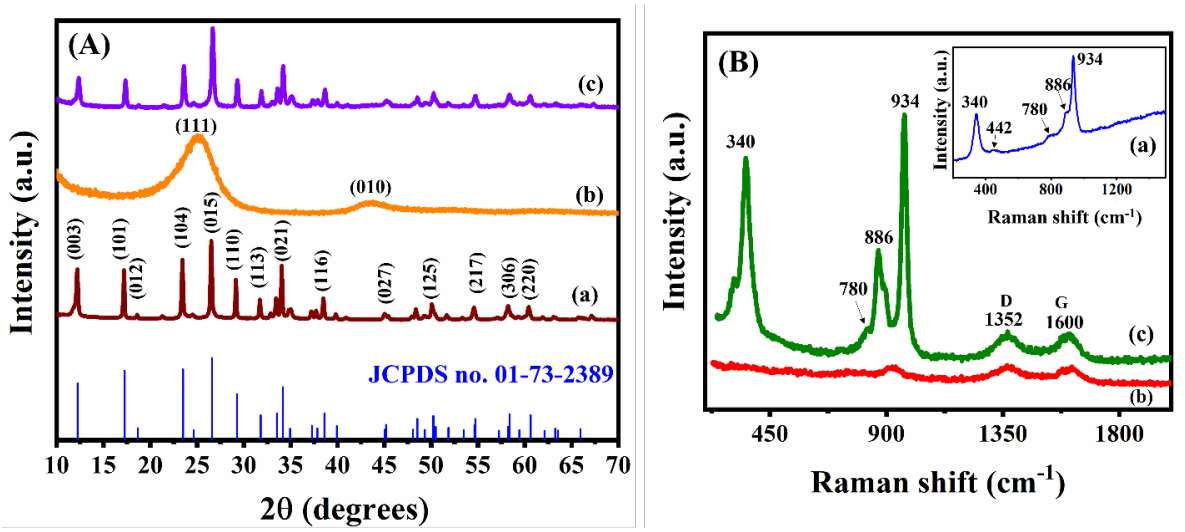

Fig. 2 A) XRD and Raman (B) spectrum of AZnMo-LDHs (a), CB (b), and AZnMo-LDHs/CB NC (c).

3.3. Oxidation state of presenting element analysis

The surface composition of AZnMo-LDHs/CB was investigated by XPS analysis to determine its chemical state constituent elements. The obtained full survey spectrum and individual high-resolution XPS spectrum are shown in Fig. 3(a-f). The full survey spectrum indicates the overall elements of Zn 2p, Mo 3d, O 1s, N 1s, and C 1s presented in appropriate binding energy values. As can be seen in our deconvoluted Zn 2p XPS spectrum, Zn^{2+} oxidation is observed at 1021.3 and 1044.5 eV for both Zn $2p_{3/2}$ and Zn $2p_{1/2}$ [36,37]. Fig. 3c illustrates the doublet peak of Mo $3d_{5/2}$ and Mo $3d_{3/2}$ at 231.3 and 234.2 eV, respectively, indicating molybdenum presenting Mo^{6+} oxidation states [38,39]. Fig. 3d shows the deconvoluted spectrum of N 1s peak fitted to the binding energy of 398.4 and 399.6 eV, attributed to N-H and N=O-C species. A successful fit of the O 1s has been obtained (see Fig. 3e) with binding energies attributed to M-O, M-O-M, and M-OH at 530.2, 531.5, and 532.7 eV, respectively [38][40]. Based on the XPS spectrum shown in Fig. 3f, C 1s have fitted with the binding energies of 284.1, 285.3, 286.6, and 288.8 eV, which corresponds to C=O, C-O, C-OH, C-N-C, and C=N, respectively [41,42]. Thus, the above results confirmed the successful integration of CB nanoparticles on AZnMo-LDHs nanoflakes structure.

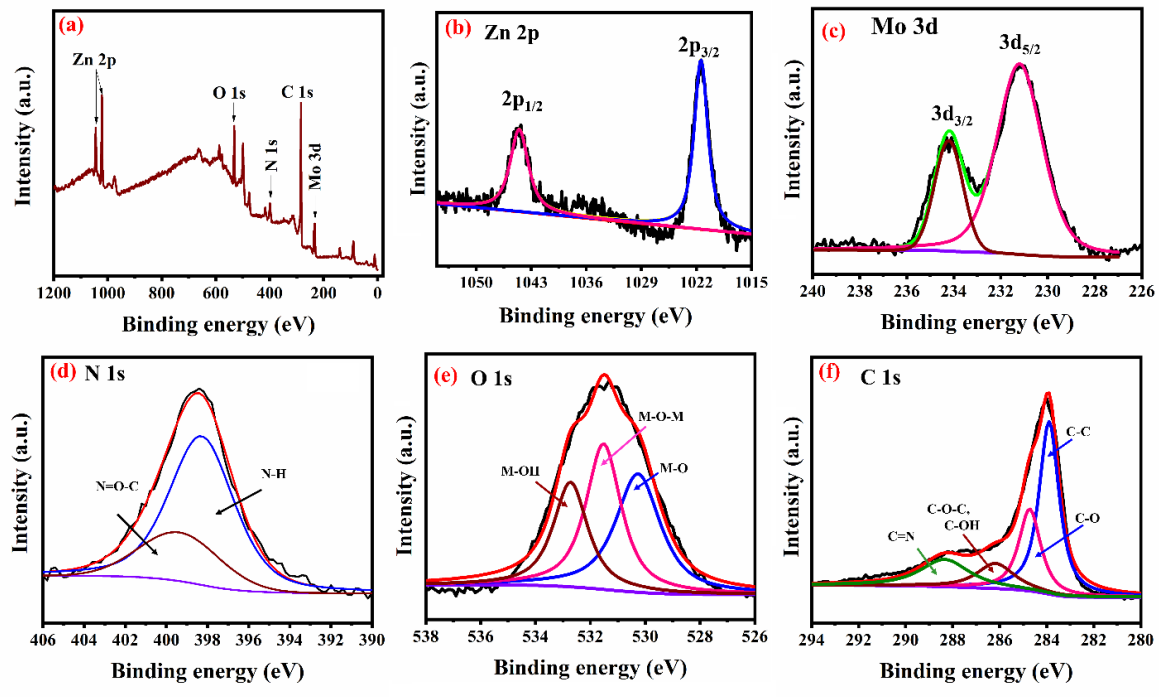

Fig. 3. Survey spectrum (a) and high-resolution XPS deconvoluted individual spectra of Zn 2p (b), Mo 3d (c), N 1s (d), O 1s (e), and C 1s (f).

3.4. Electrochemical characterization of AZnMo-LDHs/CB NC modified GCE

In electrochemical sensors, the charge transfer resistance (R_{ct}) plays an important role in electrochemical kinetics between the analyte and the electrode surface. Thus, we studied the EIS of several modified GCEs using 5 mM of $[Fe(CN)_6]^{3-/4-}$ containing 0.1 M of KCl at 100 Hz to 100 kHz. Fig. S3a shows a Nyquist plot and a Randles circuit model with R_{ct}, R_s, C_{dl}, and Z_w. In Nyquist plots, the semicircle indicates the charge transfer between electrodes and electrolyte interfaces, and the tail of the linear curve indicates diffusion-controlled channels. A bare GCE (b) had an R_{ct} of 55 Ω, indicating good contact between electrode and electrolyte species. In contrast, R_{ct} of GCE with AZnMo-LDHs increased and was determined to be 161 Ω, which resulted from electrostatic repulsion or the electrode material's low electrical conductivity. Comparatively, the R_{ct} of AZnMo-LDHs is lower than the transition metal oxide-based materials. Furthermore,

the R_{ct} was reduced to 43 Ω when the surface was modified with CB due to the surface's ionic contact and high electronic conductivity. However, the AZnMo-LDHs/CB NC/GCE demonstrated better electron transfer behavior than other modified electrodes at about R_{ct} 31 Ω, indicating excellent electron transfer properties of the composite materials. The electrochemically active surface area of the modified electrode was also analyzed using CV. Fig. S3b displays the CV response of various electrodes in 5 mM of $[Fe(CN)_6]^{3-/4-}$ with 0.1 M KCl. The CV was performed in the applied potential scanning from −0.2 to −0.6 V at a scan rate of 0.05 V/s. Comparing the results of the AZnMo-LDHs/CB NC/GCE to the response of the bare GCE, AZnMo-LDHs/GCE, and CB/GCE, it was evident that the AZnMo-LDHs/CB NC/GCE had higher peak current response with a lower peak-to-peak separation (ΔEp). The ΔEp values were calculated to be 169, 436, 147, and 73 mV for bare GCE, AZnMo-LDHs/GCE, CB/GCE, and AZnMo-LDHs/CB NC/GCE, respectively. The results show that AZnMo-LDHs/CB NC/GCE has better electrical conductivity than other modified GCEs. Fig. S3c shows that the redox peak current increases with the scan rate for AZnMo-LDHs/CB NC/GCE. Using Fig. S3d, the electrochemically active area of the AZnMo-LDHs/CB NC/GCE was calculated by the Rendles-Sevick equation [43].

The electroactive surface area values were calculated as 0.059, 0.02, 0.072, and 0.141 cm^2 for bare, AZnMo-LDHs, CB, and AZnMo-LDHs/CB NC modified GCEs, respectively. In conclusion, the as-fabricated AZnMo-LDHs/CB NC/GCE exhibit a larger electroactive surface area and a higher electrode sensitivity.

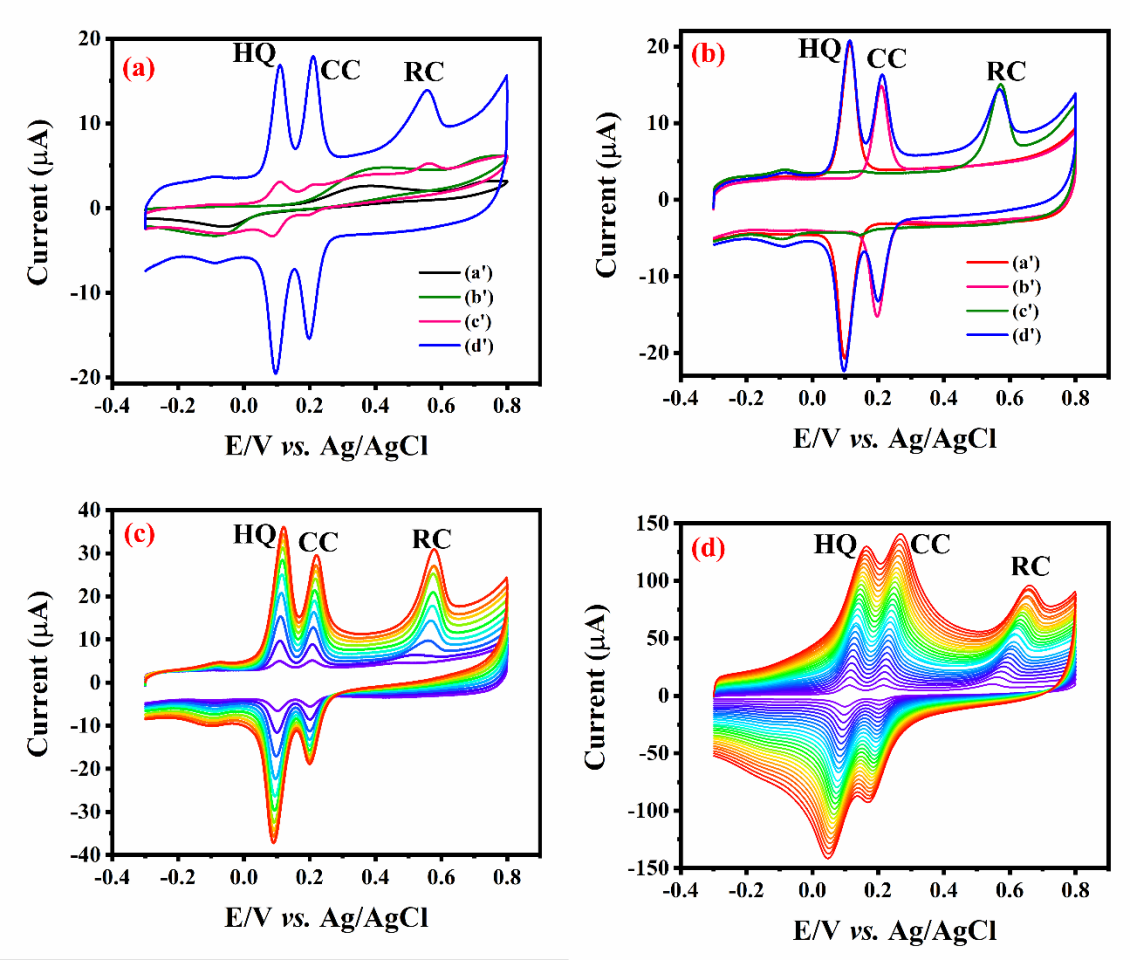

Fig. 4. a) CV response for the detection of 100 μM HQ, CC, and RC (simultaneous) using bare (a'), AZnMo-LDHs (b'), CB (c'), and AZnMo-LDHs/CB NC (d') GCEs. **b)** The CV responses for AZnMo-LDHs/CB NC modified electrode for detection of 100 μM equal concentration of HQ (a'), CC (b'), and RC (c'), and the mixture of 100 μM HQ, CC, and RC (d'). **c)** The CVs curves of AZnMo-LDHs/CB NC/GCE for simultaneous detection of HQ, CC, and RC; the concentration from 25 to 400 μM (inner to outer). **d)** The CVs were obtained for the AZnMo-LDHs/CB NC modified GCE at various scan rates from 10 to 240 mV/s (inner to outer).

Fig. 4a shows the CV response of various modified electrodes ((a') bare GCE, (b') AZnMo-LDHs/GCE, (c') CB/GCE, and (d') AZnMo-LDHs/CB NC/GCE) for detection of HQ, CC and RC in the potential scanning from -0.2 to 0.8 V at a scan rate of 50 mV/s. A single redox peak was obtained at bare GCE and AZnMo-LDHs/GCE in the presence of 100 μM HQ, CC, and RC. As the electrons move slowly between the electrolyte

and electrode interface, it could be caused by poor electrochemical activity resulting in increased overpotential. The anodic and cathodic peaks appeared at bare GCE, AZnMo-LDHs/GCE as 371, 404, and -57, -85 mV. Further, the CB-modified GCE exhibited an improved redox peak response for the presence of 100 µM HQ, CC, and RC, the corresponding redox peak potential at 107/84 mV, 216/196 mV, and 564 mV. Since carbon black has abundant electron transfer activity, the current response was smaller for detecting HQ, CC, and RC. Moreover, the as-fabricated AZnMo-LDHs/CB NC/GCE remarkably enhanced the redox peak current and reduced peak potential in the presence of 100 µM HQ, CC, and RC, the peak located at 109/97 mV, 209/199 mV, and 558 mV was revealed. The higher current and electrochemical activity response were revealed at AZnMo-LDHs/CB NC/GCE compared to all other GCEs. Synergistic interactions between AZnMo-LDHs nanoflakes and carbon block (CB) nanospheres are responsible for the higher electrochemical activity. Fig. 4b shows the CV responses of the AZnMo-LDHs/CB NC/GCE in the presence of 100 µM HQ (a') and 100 µM CC (b'), 100 µM RC (c') and simultaneous detection of 100 µM (d') HQ, CC and RC. As can be seen that a strong redox peak with peak potential differences of 13 mV and 8 mV was obtained for simultaneous detection of HQ and CC. Also, the modified electrode shows a sharp anodic peak for RC at 573 mV. A well-defined redox peak current response for HQ and CC was observed on the modified electrode. As a result of the interference of oxidative products at the surface of AZnMo-LDHs/CB NC/GCE, the oxidation peak potentials of HQ and CC were not altered. Hence, this modified electrode is more suitable for further studies. Further studies using AZnMo-LDHs/CB NC/GCE were conducted by CV to determine the electrocatalytic activity of HQ, CC, and RC at various concentrations. In Fig. 4c, HQ, CC, and RC redox current responses linearly increase with increasing HQ, CC, and RC concentrations. As a result, the concentrations of the target species (HQ, CC, and RC) are directly correlated with redox currents. The obtained linear regression equation of concentration vs. redox current of HQ and CC is (I_{pa} = 0.071x+7.54; R^2 = 0.9355 and I_{pc} = -0.0695x-9.418; R^2 = 0.9356) and (I_{pa} = 0.054x+6.597; R^2 = 0.9676 and I_{pc} = -0.0282x-7.453; R^2 = 0.903), besides, the obtained RC linear equation is y = 0.0643x+3.985; R^2 = 0.984 respectively.

An investigation of the influence of scanning rates on HQ, CC, and RC on the surface of AZnMo-LDHs/CB NC/GCE was conducted using the CV technique to clarify the kinetic processes. According to Fig. 4d, it is shown that the oxidation peak currents of RC, CC, and HQ are linearly increased as the scan speed increases from 10 to 240 mV/s. The linear equations for HQ is I_{pa} = 0.511x+6.579; R^2 = 0.9983 and I_{pc} = -0.5112x+6.579; R^2 = 0.9946, CC is Ipa = 0.473x+10.703; R^2 = 0.9921 and RS is I_{pa} = 0.327x+12.943; R^2 = 0.9901 respectively. Using this linear equation result, we conclude that the oxidation processes are typical adsorption-controlled processes with surface-confined, reversible diffusion. These results suggest that the present AZnMo-LDHs/CB NC/GCE sensor can simultaneously detect HQD, CC, and RC.

The electrochemical response of HQ, CC, and RC was also carried out on AZnMo-LDHs/CB NC/GCE by CV. Fig. S4a shows voltammograms of different concentrations of HQ in pH 7.0 at 50 mV/s scan rate. According to the CV curves, there are clearly defined cathodic and anodic peaks at potentials between 0.06 V and 0.2 V. A higher concentration of HQ and a higher linear relationship between the redox peak current and the redox peak concentration represent an increase in electron transformation properties and active electrochemical sites in the modified electrodes. In Fig. S4b, the linear calibration plot shows varying concentrations vs. redox current. The linear regression equation is I_{pa} = 0.2002x+0.2973; R^2 =0.9938 and I_{pc} = -0.1827x-1.933; R^2 =0.9957 respectively. Moreover, a scan rate study (Fig. S4c) on the measurement of (200 µM HQ) with an AZnMo-LDHs/CB NC/GCE has demonstrated that the redox peak current significantly increases with increasing the scan rates from 10 to 100 mV/s. The corresponding linear plot of different scan rates vs. redox peak currents is shown in Fig. S4d, and the corresponding linear equation is I_{pa} =0.931x+4.526; R^2 =0.9987 and I_{pc} =-0.858x-4.126; R^2 =0.9987 respectively. It is obvious from these results that HQ redox reactions are controlled through adsorption; in addition, increased scan rates were observed in parallel with increasing redox currents, indicating quasi-reversible reactions.

The electrochemical behavior of CC at an AZnMo-LDHs/CB NC/GCE was utilized to observe various concentrations from 25 to 250 µM at a 50 mV/s scan rate in PBS. As shown in Fig. S5a, upon adding 25 µM

of CC, a well-resolved redox peak concerning the increase in the CC is observed. With the increase of CC concentration from 25 to 250 µM, the CC redox signal increased linearly with the CC concentration, which can be described (shown in Fig. S5b) by an equation I_{pa} =0.1076x+3.096 with an excellent linear calibration correlation value R^2 =0.9903 and I_{pc} = -0.1052x-3.6687 correlation coefficient value R^2 =0.9902 respectively. The effect of scan rate on the redox current of CC using AZnMo-LDHs/CB NC/GCE was investigated in the presence of 200 µM CC, as shown in Fig. S5c. Furthermore, the anodic and cathodic peak current showed a linear relationship with the scan rate from 10 to 100 mV/s. With increasing scan rates, both anodic and cathodic peak currents increase proportionally. There is also a slight shift from a positive to a negative potential. Fig. S5d shows the corresponding calibration plot of the different scan rates vs. redox peak currents. The linear regression equation is I_{pa} =0.5177x+2.9413; correlation coefficient R^2 =0.9987, I_{pc} = -0.4956x-25413; R^2=0.9982 respectively. According to these results, CC's oxidation-reduction processes were adsorption-controlled electrochemical processes.

The electrochemical responses of RC were characterized using a CV to study the electrocatalytic performance of AZnMo-LDHs/CB NC/GCE. Fig. S6a shows CV curves for RC concentrations ranging from 25 to 250 M in pH 7.0 at a scan rate of 50 mV/s. The oxidation peak current of RC was increased linearly with its concentration from 25 to 250 µM. The corresponding linear regression equation is I_{pc}=0.146x+0.2087; R^2=0.993, as shown in Fig. S6b. According to this result, the RC showed higher peak current responses on AZnMo-LDHs/CB NC/GCE due to high electrocatalytic ability and large surface area of CB and AZnMo-LDHs. In addition, the influence of scan rate was explored in the range from 10 to 100 mV/s, as shown in Fig. S6c. Based on an investigation of the relationship between peak currents and scan rates, the RC oxidation peak potential shifted more positively (Fig. S6d) with the linear regression equation of I_{pa} = 0.4693x+7.264; correlation coefficient R^2 = 0.9945, indicating surface-controlled electrochemical processes.

The influence of solution pH value on the redox reaction of 100 µM mixed HQ, CC, and RC at AZnMo-LDHs/CB NC/GCE was studied by CV at 50 mV/s scan rate. As pH increases from 5 to 7, peak potential

shifts and peak currents increase (Fig. S7a), indicating that protons are involved in oxidizing HQ, CC, and RC on the modified electrode. The redox peak current dramatically decreases when pH is increased from 7 to 8. As a result, pH 7.0 was selected as the optimal pH value for HQ, CC, and RC electrochemical detection. In addition, the straight-line curve's various pH vs. oxidation peak potential was plotted as shown in Fig. S7b. The obtained calibration linear equation is E_{pa}=-0.055x+0.49; R^2 =0.9902 for HQ, E_{pa}=-0.053x+0.582; R^2=0.9979 for CC, and Epa=-0.063x+1.007; R2=0.9985 for RC respectively. A reversible electrochemical reaction with equal numbers of protons and electrons is confirmed by slope values of -0.055 and -0.053, which are close to the theoretical value of the Nernst equation (-0.059.1 V). The electrochemical oxidation reaction of RC involves the transfer of protons and electrons equally. Considering the results mentioned above, the preferred electrochemical reactions between these isomers at AZnMo-LDHs/CB NC/GCE can be described in Scheme 2.

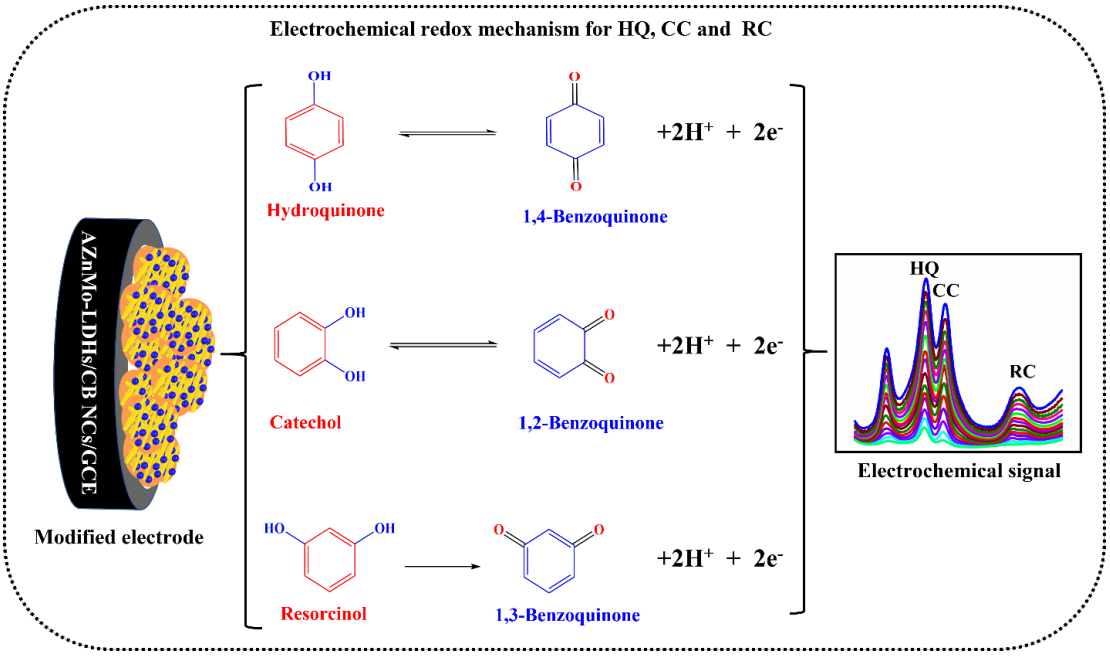

Scheme 2. The electrochemical reaction mechanism of simultaneous detection of HQ, CC, and RC at the AZnMo-LDHs/CB NC/GCE.

3.5. DPV analysis of simultaneous detection of HQ, CC, and RC

DPV was used to analyze the electrochemical performance of AZnMo-LDHs/CB NC/GCE towards HQ, CC, and RC. Fig. 5a showed the DPV curves of AZnMo-LDHs/CB NC/GCE in PBS containing 200 μM CC and RC and different concentrations of HQ (0.05–971 μM). The obtained oxidation peak current response vs. different concentrations in the range of HQ (0.05–971 μM) was plotted and displayed in Fig. 5b. The first linear range of 0.05-7.25 μM with I_{pa} = 0.538x +3.6924; R^2 = 0.9905 and the second linear range of 10.25-971.25 μM with I_{pa} =0.0364x+10.607; R^2=0.981 were obtained for detection of HQ. The lower limit of detection (LOD) was calculated using LOD = 3s/s (S/N = 3), and the calculated LOD and sensitivity were 0.00545 μM and 7.571 μA $\mu M^{-1} cm^{-1,}$ respectively. In addition, the DPV response for CC was also studied using different concentration additions in the presence of 200 μM HQ and RC. The DPV results are shown in Fig. 5c. The peak current response of CC linearly increased with the increased concentration of 0.1–103.6 μM (Fig. 5d). The linear regression equation can be written as I_{pa}= 0.00844x + 0.59222; (R^2 = 0.9951). The LOD and sensitivity were calculated for CC as 0.0018 μM and 1.142 μA μM^{-1} $cm^{-2,}$ respectively. Similarly, the HQ and CC concentrations have been fixed at 200 μM, and the DPV response of RC was studied for the various concentration additions. According to the DPV results (Fig. 5e), the concentration of RC and its broad oxidation peak current increased linearly. As obtained peak current of RC, corresponding to the first linear range (0.5-128.5 μM) of the calibration equation is I_{pa} =0.0243x+0.6224; R^2=0.9933 and the second higher linear range (148.5-1048.5 μM) of corresponding linear equation (Fig. 5f) was I_{pa} =0.0073x+3.7005; R^2=0.9706. The obtained linear equation was used to calculate the LOD and sensitivity and were 0.075 and 0.2857 μA μM^{-1} $cm^{-2,}$ respectively.

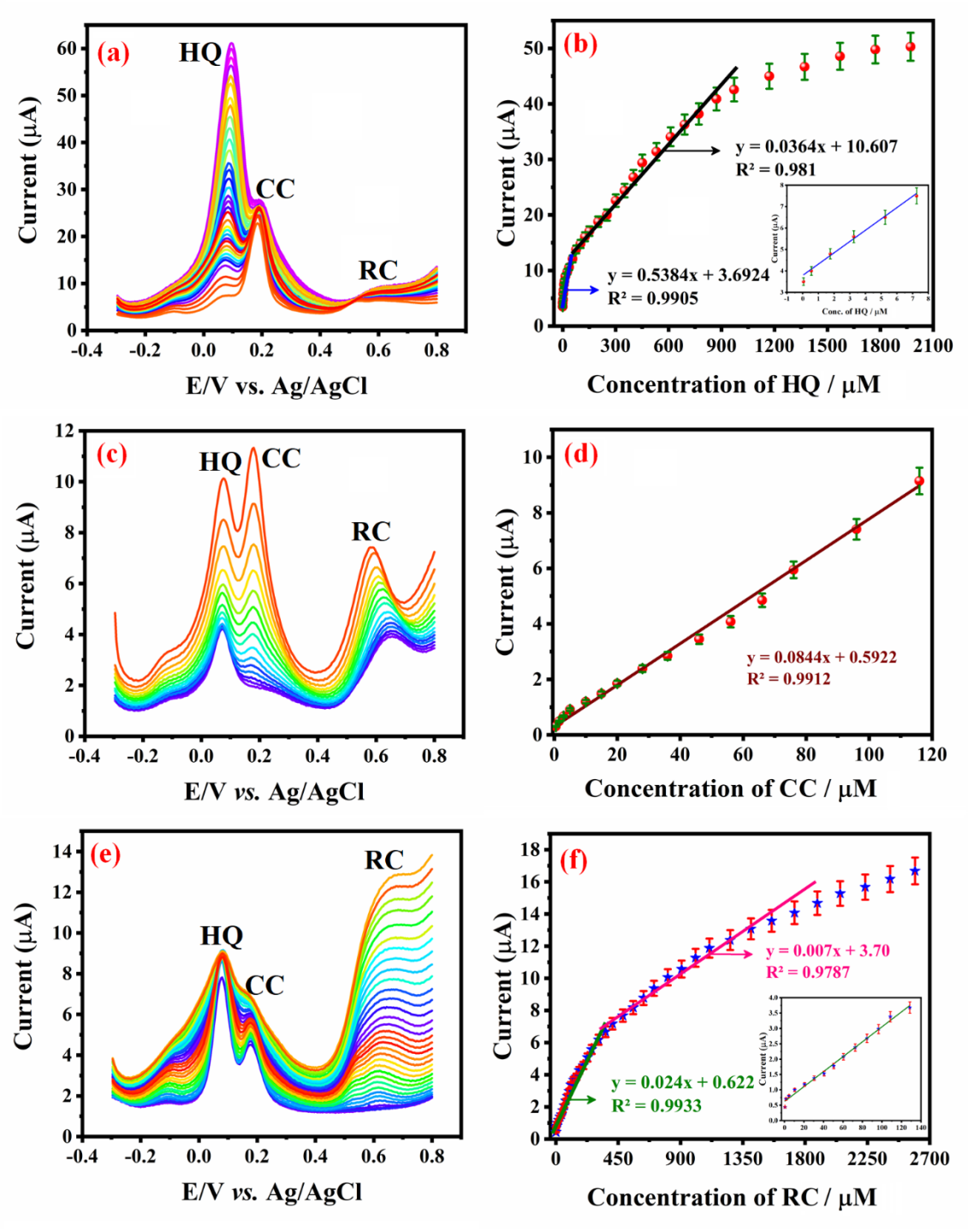

350

351 **Fig. 5. (a)** The DPV curves of AZnMo-LDHs/CB NC/GCE in various concentrations of HQ from 0.05 to 971.2

352 μM, **(b)** the corresponding linear plot of peak current vs. HQ concentration, **(c)** The DPV curves of AZnMo-

353 LDHs/CB NC/GCE for different concentration addition of CC from 0.1 to 103 μM. **(d)** The corresponding

linear plot of peak current vs. CC concentration, **(e)** The DPV curves of AZnMo-LDHs/CB NC/GCE for various concentrations of RC from 0.5 to 1408.5 µM. **(f)** The corresponding linear plot of peak current vs. RC concentration.

Fig. S8a shows the simultaneous detection of HQ, CC, and RC using AZnMo-LDHs/CB NC/GCE in pH 7.0. As the concentration of three mixers of isomers increases, the anodic peak current increases linearly. According to these results, AZnMo-LDHs/CB NC modified electrodes had a fast electrochemical activity with a facile electron movement towards the electrode interface. Due to the high synergistic effect, excellent antifouling ability, and many active sites with facile electron movement, AZnMo-LDHs/CB NC/GCE exhibit excellent catalytic activity towards simultaneous detection of HQ, CC, and RC. The comparative results are shown in **Table ST1**, which confirms that the AZnMo-LDHs/CB NC modified electrode has excellent electroanalytical performance towards HQ, CC, and RC than previously reported sensor electrodes. Also, comparative results revealed that the fabricated electrode could simultaneously be used as an advanced sensor for low-level detection of HQ, CC, and RC.

3.6. Anti-interference test, repeatability, and Reproducibility of the AZnMo-LDHs/CB NC/GCE

We have tested the anti-interference properties of the AZnMo-LDHs/CB NC/GCE in the presence of 100 µm (HQ, CC, and RC) and with 100 µm of several interfering species, including uric acid, ascorbic acid, dopamine, glucose, metal ions (Cd^{2+}, Cr^{2+}, Pb^{2+}), epinephrine, chloramphenicol, and mesalamine. In this study, the primary analytes were added together with the same amount of possible interference species; corresponding DPV analytical curves are shown in Fig. S8b. There is no existing response to the other interference peak current within 100 µm of HQ, CC, or RC of the anodic peak current, indicating excellent selectivity of AZnMo-LDHs/CB NC/GCE. Further, the repeatability test was conducted using CV on the AZnMo-LDHs/CB NC/GCE (**Fig. S10**), revealing an acceptable standard deviation (RSD) of 1.13% after eight consecutive runs. The above results confirm that the fabricated AZnMo-LDHs/CB NC/GCE can be used for

the selective and simultaneous detection of HQ, CC and RC in the presence of investigated interfering species.

3.7. Real sample analysis

We evaluated the AZnMo-LDHs/CB NC/GCE sensor's analytical applicability for simultaneous detection of HQ, CC, and RC in the water samples collected from rivers, ponds, taps, and soil. A real sample was collected from the Taipei Tamsui river, the NTUT campus, the laboratory tap water, and the neighborhood surrounding NTUT. In the first step, microparticles and harmful dust particles were removed from the collected samples, and the filtered solutions were centrifuged at 6000 rpm to obtain solutions. Afterward, the real samples were diluted ten times with PBS and analyzed as real samples. Analysis of the real sample was conducted using the standard addition method. A DPV response to different spiked water (Fig. S9 (a-c)) and soil samples (Fig. S9 (d)) revealed excellent recovery results for the real sample analysis. **Table 1** shows the concentration and recovery results of river water, pond water, tap water, and soil water samples. The excellent recoveries of HQ, CC, and RC were obtained using AZnMo-LDHs/CB NC/GCE sensor in different water and soil samples, indicating the excellent practicality of the fabricated sensor. The results also confirmed that the AZnMo-LDHs/CB NC sensor can be applied to simultaneously detect HQ, CC, and RC in environmental fluid samples.

Table 1. Determination of HQ, CC, and RC in different water and soil samples using AZnMo-LDHs/CB modified electrode.

Samples	Added (μM)			Found (μM)			Recovery (%)		
Analyte	**HQ**	**CC**	**RC**	**HQ**	**CC**	**RC**	**HQ**	**RC**	**CC**
River water	80	80	80	80.5	80	78.5	100.6	100	98.1
	100	100	100	99.6	98.6	99.4	99.6	98.6	99.4

	120	120	120	119.4	120.4	118.6	99.5	100.3	98.8
	140	140	140	138.8	139.2	139.8	99.1	99.4	99.8
Pond water	40	40	40	38.6	40.2	38.8	96.5	100.5	97
	60	60	60	60.2	58.9	58.2	100.3	98.1	97
	80	80	80	79.9	79.4	78.6	99.8	99.2	98.2
	100	100	100	99.3	98.4	99.9	99.3	98.4	99.9
	120	120	120	118.4	119.6	118.2	98.6	99.6	98.5
	140	140	140	138.6	139.4	137.6	99	99.5	98.2
	160	160	160	159.8	160.5	158.4	99.8	100.3	99
Tap water	50	50	50	48.5	49.3	48.6	97	98.6	97.2
	100	100	100	99.6	98.6	99.7	99.6	98.6	99.7
	150	150	150	149.1	148.6	149.5	99.4	99.06	99.6
	200	200	200	199.6	198.4	197.6	99.8	99.2	98.8
	250	250	250	250.3	249.8	248.3	100.1	99.92	99.32
	300	300	300	298.6	299.4	299.8	99.5	99.8	99.9
	100	100	100	98.5	100.2	98.5	98.5	100.2	98.5
Soil	200	200	200	199.4	197.8	197.6	99.7	98.9	98.8
	300	300	300	300.3	299.4	299.2	100.1	99.8	99.7
	400	400	400	398.3	398.3	399.4	99.95	99.5	99.85

397

398

399

400

4. Conclusion

In conclusion, we have developed a novel electrochemical sensor that can simultaneously determine HQ, CC, and RC using AZnMo-LDHs/CB NC modified electrodes. As a result of the high ratio surface area and good conductivity of AZnMo-LDHs/CB NC, the CB supporting AZnMo-LDHs could significantly enhance the sensitivity of the peak current response and decrease the oxidation overpotential of HQ, CC, and RC. Aside from the excellent stability and repeatability, AZnMo-LDHs/CB NC modified electrodes offer a low detection limit and a more comprehensive linear response range for determining HQ, CC, and RC. Results obtained from the application of the modified electrode to water and soil samples were satisfactory, with high recovery rates for HQ, CC, and RC. As a future possibility, AZnMo-LDHs/CB NC could be used for simultaneous detection of HQ, CC, and RC. It is also possible to use the AZnMo-LDHs/CB NC for other electrochemical sensors and energy-related applications.

Acknowledgments

The authors acknowledge the Ministry of Science and Technology, Taiwan (**MOST 110-2113-M-027-003**) for the financial support of this research. In addition, the authors also would like to thank Khalifa University, United Arab Emirates for supporting this study.

Reference

[1] S. Mu, Catechol sensor using poly (aniline-co-o-aminophenol) as an electron transfer mediator, Biosens. Bioelectron. 21 (2006) 1237–1243.

[2] Rajesh Madhu, Selvakumar Palanisamy, Shen-Ming Chen, Shakkthivel Piraman, A low temperature synthesis of activated carbon from the bio waste for simultaneous electrochemical determination of hydroquinone and catechol, Journal of Electroanalytical Chemistry 727 (2014) 84-90. https://doi.org/10.1016/j.jelechem.2014.06.005.

[3] Selvakumar Palanisamy, Chelladurai Karuppiah, Shen-Ming Chen, Cheng-Yu Yang, Prakash Periakaruppan, Simultaneous and selective electrochemical determination of dihydroxybenzene isomers at a reduced graphene oxide and copper nanoparticles composite modified glassy carbon electrode, Anal. Methods, 6 (2014) 4271-4278 https://doi.org/10.1039/C4AY00433G.

[4] J. Yu, W. Du, F. Zhao, B. Zeng, High sensitive simultaneous determination of catechol and hydroquinone at mesoporous carbon CMK-3 electrode in comparison with multi-walled carbon nanotubes and Vulcan XC-72 carbon electrodes, Electrochim. Acta. 54 (2009) 984–988.

[5] T.S.S.K. Naik, A.V. Kesavan, B.E.K. Swamy, S. Singh, A.G. Anil, V. Madhavi, P.C. Ramamurthy, Low cost, trouble-free disposable pencil graphite electrode sensor for the simultaneous detection of hydroquinone and catechol, Mater. Chem. Phys. 278 (2022) 125663.

[6] L. Zheng, L. Xiong, Y. Li, J. Xu, X. Kang, Z. Zou, S. Yang, J. Xia, Facile preparation of polydopamine-reduced graphene oxide nanocomposite and its electrochemical application in simultaneous determination of hydroquinone and catechol, Sensors Actuators B Chem. 177 (2013) 344–349.

[7] Y.-G. Sun, H. Cui, Y.-H. Li, X.-Q. Lin, Determination of some catechol derivatives by a flow injection electrochemiluminescent inhibition method, Talanta. 53 (2000) 661–666.

[8] G.K.-J. Chao, J.C. Suatoni, Determination of phenolic compounds by HPLC, J. Chromatogr. Sci. 20 (1982) 436–440.

[9] P. Nagaraja, R.A. Vasantha, K.R. Sunitha, A new sensitive and selective spectrophotometric method for the determination of catechol derivatives and its pharmaceutical preparations, J. Pharm. Biomed. Anal. 25 (2001) 417–424.

[10] V. Rives, M.A. Ulibarri, Layered double hydroxides (LDH) intercalated with metal coordination compounds and oxometalates, Coord. Chem. Rev. 181 (1999) 61–120.

[11] Q. Wang, D. O'Hare, Recent advances in the synthesis and application of layered double hydroxide (LDH) nanosheets, Chem. Rev. 112 (2012) 4124–4155.

[12] N. Baig, M. Sajid, Applications of layered double hydroxides based electrochemical sensors for determination of environmental pollutants: a review, Trends Environ. Anal. Chem. 16 (2017) 1–15.

[13] S. Lei, K. Tang, Q. Liu, Z. Fang, Q. Yang, H. Zheng, Preparation of manganese molybdate rods and hollow olive-like spheres, J. Mater. Sci. 41 (2006) 4737–4743.

[14] Z. Zhao, Y. Sun, J. Song, Y. Li, Y. Xie, H. Cui, W. Gong, J. Hu, Y. Chen, Highly sensitive nonenzymetic glucose sensing based on multicomponent hierarchical NiCo-LDH/CCCH/CuF nanostructures, Sensors Actuators B Chem. 326 (2021) 128811.

[15] H. Xia, Q. Xu, J. Zhang, Recent Progress on Two-Dimensional Nanoflake Ensembles for Energy Storage Applications, Nano-Micro Lett. 10 (2018) 66. https://doi.org/10.1007/s40820-018-0219-z.

[16] C. Karuppiah, S.M. Babulal, T-W. Chen, S-M. Chen, L-F. Hsu, D.A.A. Farraj, S.K. Ramaraj, M. S. Elshikh, C-C. Yang, A novel ammonium zinc molybdate layered double hydroxide nanoflakes/vapor grown carbon fibers nanomaterials based electrocatalyst for the monitoring of dimetridazole drug in real samples, J. .Environ. Chem. Eng., 10 (2022) 108227.

[17] R. Xiao, S. Wang, M.H. Ibrahim, H.I. Abdu, D. Shan, J. Chen, X. Lu, Three-dimensional hierarchical frameworks based on molybdenum disulfide-graphene oxide-supported magnetic nanoparticles for enrichment fluoroquinolone antibiotics in water, J. Chromatogr. A. 1593 (2019) 1–8.

[18] W. Zhang, Q. Liu, P. Chen, Flexible strain sensor based on carbon black/silver nanoparticles

composite for human motion detection, Materials (Basel). 11 (2018) 1836.

[19] F.C. Vicentini, A.E. Ravanini, L.C.S. Figueiredo-Filho, J. Iniesta, C.E. Banks, O. Fatibello-Filho, Imparting improvements in electrochemical sensors: evaluation of different carbon blacks that give rise to significant improvement in the performance of electroanalytical sensing platforms, Electrochim. Acta. 157 (2015) 125–133.

[20] F. Arduini, C. Majorani, A. Amine, D. Moscone, G. Palleschi, Hg2+ detection by measuring thiol groups with a highly sensitive screen-printed electrode modified with a nanostructured carbon black film, Electrochim. Acta. 56 (2011) 4209–4215.

[21] Selvakumar Palanisamy, Chelladurai Karuppiah, Shen-Ming Chen, K Muthupandi, R Emmanuel, P Prakash, Mohamed S Elshikh, M Ajmal Ali, Fahad MA Al-Hemaid, Selective and simultaneous determination of dihydroxybenzene isomers based on green synthesized gold nanoparticles decorated reduced graphene oxide, Electroanalysis 27 (2015) 1144-1151. https://doi.org/10.1002/elan.201400657.

[22] S. Palanisamy, A.T. Ezhil Vilian, S.M. Chen, Direct electrochemistry of glucose oxidase at reduced graphene oxide/zinc oxide composite modified electrode for glucose sensor, Int. J. Electrochem. Sci. 7 (2012) 2153–2163.

[23] J. Ahmed, M. Faisal, M. Jalalah, M. Alsaiari, S.A. Alsareii, F.A. Harraz, An efficient amperometric catechol sensor based on novel polypyrrole-carbon black doped α-Fe2O3 nanocomposite, Colloids Surfaces A Physicochem. Eng. Asp. 619 (2021) 126469. https://doi.org/https://doi.org/10.1016/j.colsurfa.2021.126469.

[24] T. Zhang, H. Guo, M. Yang, L. Sun, J. Zhang, M. Wang, F. Yang, N. Wu, W. Yang, Electrochemical sensor based on UiO-66-NH2/COCl-MWCNT/CB for simultaneous detection of dihydroxybenzene isomers in different water samples, Microchem. J. 175 (2022) 107139.

https://doi.org/https://doi.org/10.1016/j.microc.2021.107139.

[25] F. Arduini, C. Zanardi, S. Cinti, F. Terzi, D. Moscone, G. Palleschi, R. Seeber, Effective electrochemical sensor based on screen-printed electrodes modified with a carbon black-Au nanoparticles composite, Sensors Actuators B Chem. 212 (2015) 536–543. https://doi.org/https://doi.org/10.1016/j.snb.2015.02.051.

[26] Y. Wei, C. Gao, F.-L. Meng, H.-H. Li, L. Wang, J.-H. Liu, X.-J. Huang, SnO2/reduced graphene oxide nanocomposite for the simultaneous electrochemical detection of cadmium (II), lead (II), copper (II), and mercury (II): an interesting favorable mutual interference, J. Phys. Chem. C. 116 (2012) 1034–1041.

[27] P. Batista Deroco, F. Campanhã Vicentini, O. Fatibello-Filho, An electrochemical sensor for the simultaneous determination of paracetamol and codeine using a glassy carbon electrode modified with nickel oxide nanoparticles and carbon black, Electroanalysis. 27 (2015) 2214–2220.

[28] K.A. Béres, I.E. Sajó, G. Lendvay, L. Trif, V.M. Petruševski, B. Barta-Holló, L. Korecz, F.P. Franguelli, K. László, I.M. Szilágyi, Solid-Phase “Self-Hydrolysis” of [Zn (NH3) 4MoO4@ 2H2O] Involving Enclathrated Water—An Easy Route to a Layered Basic Ammonium Zinc Molybdate Coordination Polymer, Molecules. 26 (2021) 4022.

[29] A.K. Choudhary, H. Pramanik, Synthesis of low-cost HNO3-functionalized acetylene black carbon supported Pt-Ru/CAB nano electrocatalysts for the application in direct ethanol fuel cell (DEFC), Korean J. Chem. Eng. 36 (2019) 1688–1707. https://doi.org/10.1007/s11814-019-0343-6.

[30] B.J. Reddy, P. Vickraman, A.S. Justin, A facile synthesis of novel $$\upalpha $$ α-$$\hbox {ZnMoO} _ {{4}} $$ ZnMoO 4 microspheres as electrode material for supercapacitor applications, Bull. Mater. Sci. 42 (2019) 1–6.

[31] H. Liu, C. Yin, H. Zhang, C. Liu, Sustainable synthesis of ammonium nickel molybdate for hydrodesulfurization of dibenzothiophene, Chinese J. Catal. 37 (2016) 1502–1511.

[32] Y.-P. Gao, K.-J. Huang, C.-X. Zhang, S.-S. Song, X. Wu, High-performance symmetric supercapacitor based on flower-like zinc molybdate, J. Alloys Compd. 731 (2018) 1151–1158.

[33] D. Carriazo, C. Domingo, C. Martin, V. Rives, Structural and texture evolution with temperature of layered double hydroxides intercalated with paramolybdate anions, Inorg. Chem. 45 (2006) 1243–1251.

[34] L. Bokobza, J.-L. Bruneel, M. Couzi, Raman spectroscopic investigation of carbon-based materials and their composites. Comparison between carbon nanotubes and carbon black, Chem. Phys. Lett. 590 (2013) 153–159.

[35] M. Pawlyta, J.-N. Rouzaud, S. Duber, Raman microspectroscopy characterization of carbon blacks: Spectral analysis and structural information, Carbon N. Y. 84 (2015) 479–490.

[36] A.B. Appiagyei, J.O. Bonsu, J.I. Han, Robust structural stability and performance-enhanced asymmetric supercapacitors based on CuMoO4/ZnMoO4 nanoflowers prepared via a simple and low-energy precipitation route, J. Mater. Sci. Mater. Electron. 32 (2021) 6668–6681. https://doi.org/10.1007/s10854-021-05382-y.

[37] J. Anupriya, Facile Hydrothermal Synthesis of Cubic Zinc Ferrite Nanoparticles for Electrochemical Detection of Anti- inflammatory Drug Nimesulide in Biological and Pharmaceutical Sample, Int. J. Electrochem. Sci. 16 (2021) ArticleID:210772. https://doi.org/10.20964/2021.07.72.

[38] J. Wang, H. Yan, W. Hu, Preparation and inhibition behavior of molybdate intercalated ZnAlCe-hydrotalcite, J. Chinese Soc. Corros. Prot. 36 (2016) 637–644. https://doi.org/10.11902/1005.4537.2016.186.

[39] Q. Cao, L. Zhao, A. Wang, L. Yang, L. Lai, Z.L. Wang, J. Kim, W. Zhou, Y. Yamauchi, J. Lin, Tailored synthesis of Zn-N co-doped porous MoC nanosheets towards efficient hydrogen evolution, Nanoscale. 11 (2019) 1700–1709. https://doi.org/10.1039/c8nr07463a.

[40] Y. Xu, T. Liu, Y. Li, Y. Liu, F. Ge, Nanostructure design and catalytic performance of Mo/ZnAl-LDH in

cationic orchid X-BL removal, Materials (Basel). 11 (2018). https://doi.org/10.3390/ma11122390.

[41] G. George, M.P. Saravanakumar, Facile synthesis of carbon-coated layered double hydroxide and its comparative characterisation with Zn–Al LDH: application on crystal violet and malachite green dye adsorption—isotherm, kinetics and Box-Behnken design, Environ. Sci. Pollut. Res. 25 (2018) 30236–30254. https://doi.org/10.1007/s11356-018-3001-3.

[42] H. Han, J. Lee, D.W. Park, S.E. Shim, Surface modification of carbon black by oleic acid for miniemulsion polymerization of styrene, Macromol. Res. 18 (2010) 435–441. https://doi.org/10.1007/s13233-010-0505-1.

[43] D. Salinas-Torres, F. Huerta, F. Montilla, E. Morallón, Study on electroactive and electrocatalytic surfaces of single walled carbon nanotube-modified electrodes, Electrochim. Acta. 56 (2011) 2464–2470. https://doi.org/https://doi.org/10.1016/j.electacta.2010.11.023.